Fuel 371 (2024) 132096

Contents lists available at ScienceDirect

Fuel

journal homepage: www.elsevier.com/locate/fuel

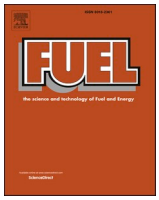

Full Length Article

Insights into pyrolysis product characteristics and carbon structure evolution of bituminous coal under high-temperature thermal shock

Haigang Zhang [a,b], Zhongjie Shen [a,b,*], Rubin Zeng [a,b], Qinfeng Liang [a,b], Haifeng Liu [a,b]

[a] National Energy Coal Gasification Technology Research and Development Center, East China University of Science and Technology, P.O. Box 272, Shanghai 200237, PR China

[b] Shanghai Engineering Research Center of Coal Gasification, East China University of Science and Technology, P.O. Box 272, Shanghai 200237, PR China

ARTICLE INFO

Keywords:
High-temperature pyrolysis
Thermal shock
Product distribution
Carbon nanostructure
Carbonization

ABSTRACT

The current investigation aims to reveal the pyrolysis characteristics and particle microstructure evolution of bituminous coal under the high-temperature thermal shock. In the experimental temperatures, the purification of carbon matrix in the coal char is a successive process linear on temperature. In contrast, the graphitization process of carbon structure existed a transition temperature (1600 ℃). Specifically, the range of 1000–1500 ℃ is critical for the transformation of amorphous carbon to disordered graphite, but the growth of graphite microcrystals was minimally affected. While the range of 1600–1900 ℃ is critical for the formation of the graphite-like carbon structure. It is characterized by the release of defective structures such as oxygen-containing functional groups, and a significant increase in crystal size. Although beneficial for the subsequent study of carbon materials, the ordered graphite transformation led to the deactivation of char. The pyrolysis behavior study under thermal shock insight into the thermal behavior of coal char in high-temperature furnaces, as well as a new idea for the clean utilization of coal resources.

1. Introduction

Currently, coal is still an essential industrial raw material and energy source, and is widely employed in processes such as combustion, gasification, metallurgy coking, and carbon materials manufacturing. Under the requirement of carbon neutrality policy, the efficient conversion and clean utilization of raw coal still have certain urgency and necessity [1]. Within the gasifier or furnace, the thermal behavior of coal in the high-temperature area significantly impacts equipment operations, in addition to directly affecting char utilization efficiency and industrial energy consumption, as the high-temperature results in the formation of molten slag and reduction of carbon activity [2]. Given the scarcity of high-quality coal resources, and increased environmental and economic pressures, enhancing the reaction performance of coal char to ensure complete conversion becomes necessary, as it is related to the industrial coal consumption and residual carbon formation in the slag. However, the carbon structure of coal char in the furnace is the basic factor in determining the reaction performance [3,4].

As coal particle is introduced into a high-temperature area of industrial furnaces, the particles undergo rapid pyrolysis and carbonization due to the impact of flame and high-temperature thermal shock, leading to the formation of a distinct structure in coal char [5,6]. The char structure and composition presented a different property from that of raw coal, which leads to a loss of reactivity [7,8]. This phenomenon is called “thermal annealing” or “thermal deactivation” in industry [9]. The high-temperature areas (>1000 ℃) of these industrial furnaces encompass the flame zone of the boiler, the combustion and carbonization chambers of the coke oven, and the combustion area of the entrained flow gasifier, etc. The carbon property in the coal char demonstrates a reduced disorder at high temperatures and the increased graphitization degree significantly influences the release of pyrolysis products and the gasification or combustion reactivity, leading to the formation of residual carbon in slag and overall coal conversion [10,11]. Yu et al. [12] found that the coal char gasification reactivity index was linearly and negatively correlated with the Raman structural parameter characterizing the degree of graphitization, and the difference in graphitization between different coals decreased as the temperature increased. While, Xu et al. [13] found that the elevated degree of graphitization in coal char leads to the formation of a large number of polycyclic aromatic hydrocarbons (PAHs) with reduced aliphatic side chains, concurrently enhancing gas-phase products yield. Despite numerous studies exploring the impact of pyrolysis conditions on coal

* Corresponding author.
E-mail address: zjshen@ecust.edu.cn (Z. Shen).

https://doi.org/10.1016/j.fuel.2024.132096
Received 26 January 2024; Received in revised form 17 May 2024; Accepted 2 June 2024
Available online 8 June 2024

char reactivity, understanding the coal char aromatization process and its influencing factors under high-temperature conditions, particularly in the flame area (1000–1900 ℃), remains incomplete [14,15]. The investigation of carbon structure evolution in coal char under high-temperature conditions can help utilize its special properties, enhancing coal char utilization and economic benefits.

Temperature is the pivotal factor influencing the transformation of the carbon structure, particularly in high-temperature [16,17]. When coal particles are injected into the high-temperature flame area, rapid carbonization and impurity element elimination occur, alongside the speedy formation of aromatic compounds [18]. However, insufficient investigation focuses on the pyrolysis characteristics and carbon crystal structure alterations in coal char during this temperature stage. Some studies suggest an increase in crystal size at this stage [19,20], while other work proposes that it represents a stage of aromatization [21,22]. Meanwhile, due to the non-homogeneity, several significant questions remain unsolved during the high-temperature pyrolysis stage, such as the formation of carbon skeleton and the conditions affecting carbonization during this stage [2,23]. Consequently, a thorough exploration of coal char composition and structural variation during the high-temperature stage is essential, the relationship between carbon structure and pyrolysis temperature needs to be established to rationally regulate the properties of coal char such as strength and reactivity.

In addition, the utilization of coal char has garnered significant attention in the production of carbon materials due to its lower H/C ratio in recent years and has become a hotspot in current research [24,25]. The presence of aromatic layers and aliphatic chains in coal naturally makes it a desirable raw material for the manufacturing of various coal-based carbon materials. Generally, the coal-to-graphite process is divided into two distinct stages: carbonization (<2000 ℃) and graphitization (>2000 ℃) [2]. The carbonization process involves the removal of heteroatoms and the formation of an aromatic carbon skeleton in the graphitized carbonaceous material, whereas the graphitization process mainly involves the further condensation of the aromatic carbon layer and its structural rearrangement to form a tricycle graphite structure [26,27]. Pyrolysis is the key initial step in the thermochemical transformation process, but the previous studies mainly focused on the growth of microcrystalline structure and the evolution of structural defects in the graphitization stage, and limited studies can explain in detail the transformation of microscopic amorphous carbon and composition variation of the raw materials in the carbonization stage [25]. The study focused on the evolution of carbon structure in this temperature range can also facilitate to optimization of the temperature control strategy in the preparation of coal-based carbon materials in the future.

In this study, the product release pattern and char structure evolution process during pyrolysis of bituminous coal under thermal shock at 1000–1900 ℃ were investigated. Pyrolysis of coal samples at different temperatures was realized with a modified flash Joule heating equipment, and the gas components of the collected samples were analyzed using gas chromatography. The impact of thermal shock on the surface structure of coal char was examined through scanning electron microscopy (SEM). Besides, a comprehensive and meticulous study of the carbon structure evolution in the coal char and the growth process of graphite microcrystals within the temperature range was conducted by multiple characterization methods, including XRD, Raman spectroscopy, and TEM. The critical temperature range for microcrystal growth was obtained. The results are important for regulating the degree of graphitization and enhancing the reactivity of coal char in the furnace.

2. Material and methodology

2.1. Materials

The experimental raw material used in this study was Yili bituminous coal (Xinjiang, China). After drying, the samples were crushed and screened, and the particles with a size of 0.8–1.25 mm were selected as pyrolysis feedstock for pyrolysis in this experiment. In industrial boilers and coke ovens, the size requirement for coal particles is typically in the millimeter range, aimed at minimizing the generation of fine ash dust and ensuring combustion stability [28,29]. While, for the entrained flow gasifier, to maintain a high gasification conversion, the particle size requirement is less than 100 μm[30]. In this experiment, a novel approach was used to heat coal particles by directly passing through a high electric current, which could rapidly generate the Joule heat within the particle for uniform heating, and eliminate variations in the pyrolysis product distribution resulting from differences in heat transfer associated with particle size changes.

The proximate and ultimate analyses were performed on a 5E-MACIII (Kaiyuan company, China) and a Vario MACRO element analyzer (Elementar, Germany), and the results are shown in Table 1.

The ash sample was obtained after the raw coal was completely combusted at 815 °C. The chemical composition was analyzed by Advant'X Intellipower^{TM} 3600 X-ray fluorescence (XRF, Thermo Fisher Scientific, America). The composition is shown in Table 2. Additionally, the ash melting temperatures (AFTs) were determined by the 5E-AF4000 ash melting point tester (Kaiyuan, China), and the results are presented in Table 2. The deformation temperature (DT) is 1310 ℃, while the flow temperature (FT) is 1334 °C, proving the low flowability of coal ash. The high content of acid oxides in the coal ash determined its higher melting point.

2.2. Pyrolysis experimental method

The pyrolytic carbonization experiments of bituminous coal were carried out under N_2 atmosphere in a modified flash Joule heating equipment and the schematic diagram is shown in Fig. 1(a). Before the experiment, about 1.0 g of raw coal particles were placed within a graphite crucible, and the crucible was fixed in a copper injection mold. Cooling water was circulated inside the mold to prevent excessive heat. During the experiment, a specific voltage was applied at both ends of the copper injection mold to generate sufficient Joule heat within the graphite crucible. A direct current (DC) of about 500A flowed through the graphite crucible and coal particles were rapidly heated to the experimental temperature within seconds. The voltage was then adjusted to maintain the samples at the experimental temperature for about 15 s with a deviation of 3 s. Subsequently, the samples were analyzed after cooling to room temperature. Each set of experiments was repeated three times, and the particle temperature was determined by the corrected infrared thermometer above the equipment. The pyrolysis gas was collected into a gas bag and the composition was determined using a portable gas chromatograph (Agilent 990 Micro GC, USA).

2.3. Analytical method

Crystal structure information in the samples was obtained by PANalyticalX'pert Powder X-ray powder diffractometer (XRD) with Cu Kα radiation (ThermoFisher Scientific, America). Further, detailed carbon peak information was obtained by PeakFit software fitting. According to the XRD results, the (002) peak of the sample can be divided into two Gaussian peaks at about 22.4° (γ peak) and 25.5° ((002) peak), and the area of the (100) peak was also obtained by Gaussian fitting. The integral areas of the (002) and γ peaks obtained by fitting represent the relative contents of aromatic carbon atoms (C_{ar}) and aliphatic carbon atoms (C_{al}), respectively. After that, the carbon structural parameters, including the aromaticity (f_a), interlayer spacing (d_{002}), stacking height (L_c), crystallite lateral size (L_a), and stacked layers (n), were obtained based on the following formulas [2,31].

$$f_a = C_{ar}/(C_{ar} + C_{al}) = A_{002}/(A_{002} + A_\gamma) \quad (1)$$

$$d_{002} = \lambda/(2\sin\theta_{002}) \quad (2)$$

Table 1
Proximate and ultimate analyses(wt.%) of bituminous coal used in this study.

Proximate analysis (d, wt. %)				Ultimate analysis (daf, wt. %)				
Components	V	FC	A	C	H	S	N	O
Yili coal	31.95	57.78	10.27	75.64	3.97	1.45	1.24	17.71

* The oxygen content was obtained by difference.

Table 2
Chemical compositions (wt.%) and ash fusion temperature of coal ash.

	Component content(wt.%)								
	SiO_2	CaO	Al_2O_3	Fe_2O_3	K_2O	TiO_2	MgO	Na_2O	Others
Yili-Ash	45.40	14.76	17.25	12.75	0.88	0.92	3.03	0.72	4.29
	DT (℃)		ST (℃)		HT (℃)			FT (℃)	
Yili-Ash	1286		1291		1295			1308	

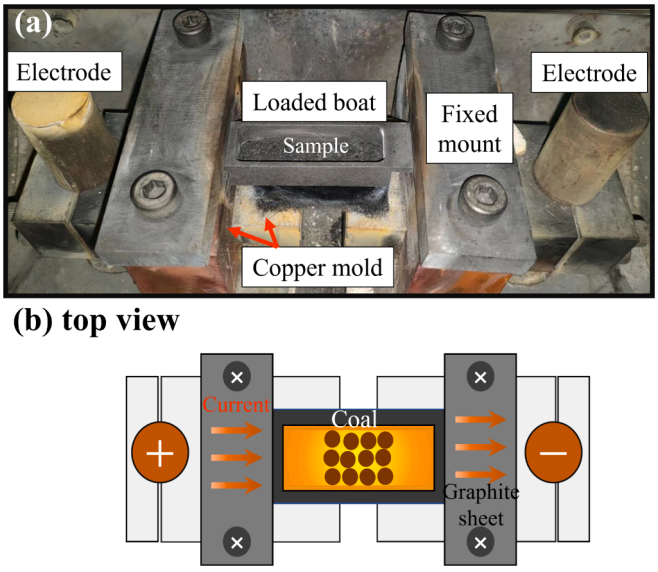

Fig. 1. Schematic diagram of the flash Joule heating process, (a) set-up picture; (b) top view schematic.

$$L_a = 1.84\lambda/(\beta_{100}\cos\theta_{100}) \quad (3)$$

$$L_c = 0.89\lambda/(\beta_{002}\cos\theta_{002}) \quad (4)$$

where λ is the X-ray wavelength, $\lambda = 0.15406$ nm; β and θ are the full width at half-maximum (FWHM) and diffraction angle, respectively.

For the carbon structure and composition structural analysis of char, the laser wavelength used for Raman spectroscopy (ThermoFisher Scientific, America) was 432 nm. The Raman spectra were further deconvoluted into D and G peaks to obtain the hidden carbon structure information by Origin software. The average lateral size (L_a) of the microcrystals was calculated by the Eq. (5) [32]:

$$L_a = \frac{C_0 + C_1\lambda_L}{I_{D_1}/I_G} \quad (5)$$

where C_0 and C_1 are the structural parameters, $C_0 = -12.6$ nm and $C_1 = 0.033$ nm [16]; λ_L is the laser wavelength; I_{D1} and I_G are the peak areas.

The sample microstructure was characterized by the transmission electron microscope (TEM, Talos F200X, America), and the resulting images were processed using Gatan DigitalMicrograph software, following established methods in the literature [2,33]. The method facilitated the analysis of the structural information of graphite layers in the pyrolysis char, including layer spacing. Additionally, the surface morphology was examined using a scanning electron microscope (SEM, Hitachi SU1510, Japan). The specific surface area and pore volume were determined by nitrogen adsorption/desorption isotherm experiments by the specific surface area analyzer (Qantachrom Corp, USA) at 77 K, and further calculated according to the Barret- Joyner-Helena method (BJH) [34].

3. Results and discussion

3.1. Pyrolysis product

Temperature plays a crucial role in influencing the release and distribution of pyrolysis products [13,35]. Previous studies have demonstrated that rapid pyrolysis of high-rank coal at temperatures exceeding 1000 ℃ results in the predominant formation of gas and coal char, accompanied by a minimal tar content (<2%) [36,37]. As the temperature rises (>800 ℃), the yield of tar consistently declines [36], and given the specific high-temperature pyrolysis conditions, this study focuses on the examination of the coal char characteristics and pyrolysis gas composition.

The composition of pyrolysis gas products resulting from the thermal shock of coal at various high temperatures is presented in Fig. 2. The primary constituents of the pyrolysis gas include H_2, CO, and CO_2, with minor quantities of CH_4 and ethylene. Notably, in contrast to the gas product composition obtained through the conventional pyrolysis process [38], the pyrolysis gas produced by rapid thermal shock exhibited a significantly higher proportion of syngas (CO + H_2), reaching 90 %. Methane primarily arose from the demethylation reaction occurring in the aromatic side chains, while, higher temperatures will lead to the complete fragmentation of carbon-hydrogen bonds present in aliphatic compounds or side chains. Consequently, the pyrolysis gas exhibited a low concentration of methane and ethylene, while displaying a high hydrogen content. With an increase in the pyrolysis temperature, especially above 1500 ℃, the gas composition experienced a substantial rise in CO content, accompanied by a significant decrease in CO_2. CO_2 mainly comes from the cleavage of –COOH, which is entirely broken at lower temperatures (<900 ℃). In contrast, carbonyl and heterocyclooxy functional groups serve as the primary sources of CO in pyrolysis gases, requiring higher activation energies to break compared to the carboxyl group. Consequently, higher pyrolysis temperatures are necessary for the complete breakdown of these functional groups, resulting in an elevated CO content and decreased CO_2 content in the gas-phase products at higher temperatures. Meanwhile, higher pyrolysis temperatures enhance the reaction rate of coal char, and the char is more likely to gasify with CO_2, which consumes a portion of the CO_2 generated. Besides, carbothermal reactions with minerals at higher temperatures also

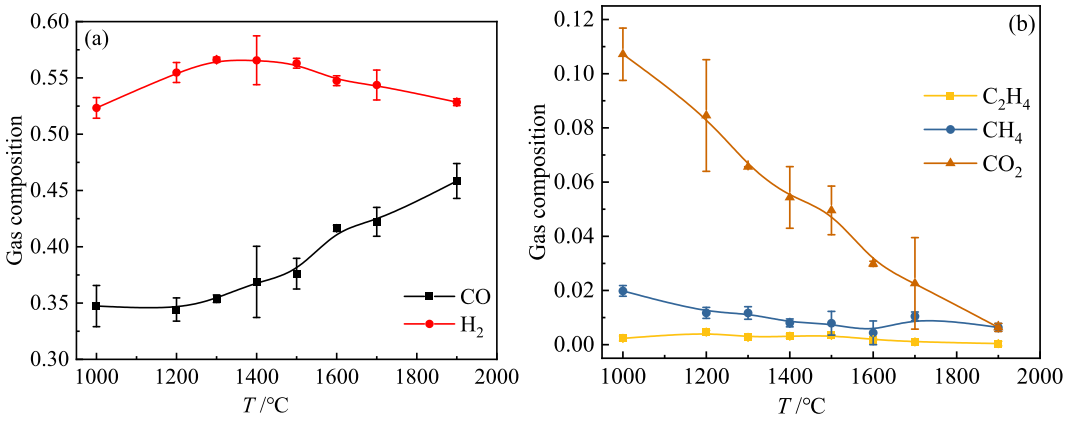

Fig. 2. Distribution of pyrolysis gas composition under different temperatures.

contribute to CO production [39]. Further, by raising the reaction temperature, the concentration of syngas can be increased to over 95 %.

Fig. 3 shows the composition and elemental content results of pyrolysis char at various temperatures. In Fig. 3(a), a notable decrease in volatile content and an increase in fixed carbon content were observed during pyrolysis carbonization of coal at 1000 ℃ thermal shock, as compared to the raw coal composition results in Table 1. As the temperature increased, the precipitation of volatiles was further promoted. Between 1000–1600 ℃, the volatile content continued to decrease while reaching higher temperatures (>1700 ℃) resulting in basically complete release. Simultaneously, the reduction in volatile content also led to an increase in relative ash content. However, a noteworthy point is the decline in fixed carbon content above 1400 ℃, mainly manifested as a decrease in the oxygen content, which can be attributed to the occurrence of condensation reactions and the formation of graphite microcrystals during high-temperature carbonization. Moreover, in this study, the ash tracer method was employed to estimate the release of volatiles (R_V) and quantify the impact of reaction temperature on the extent of pyrolysis [37]. The calculation is shown in Eq. (6):

$$R_V = \frac{V_0 - \frac{A_0}{A}V}{V_0} \times 100\% \quad (6)$$

where V_0 and A_0 are the volatiles and ash content of raw coal respectively; V and A are the corresponding components in char.

The results of volatile release (R_V) are shown in Fig. 3(a). At 1000 ℃, R_V remained below 80 %, indicating incomplete release of volatiles in the raw coal during the thermal shock process. Nevertheless, temperature significantly influences the promotion of volatile release. As the temperature rises from 1200 to 1700 ℃, the volatile fraction release rate exhibited a linear increase, reaching over 98.8 %.

The elements (C, H, O, N, S) composition results of residual char measured on the dry ash-free (daf) basis are shown in Fig. 3(b). As the temperature rose, the carbon (C) element monotonically increased, while the content of hydrogen (H), oxygen (O), and nitrogen (N) progressively decreased. The enrichment of carbon content primarily occurred within the temperature range of 1000–1200 ℃ and above 1500 ℃, with minimal changes observed between 1200–1500 ℃. A comparison of the remaining elements showed that the increase in the relative content of carbon within the range of 1000–1200 ℃ can be attributed to the release of hydrogen (H), sulfur (S), and nitrogen (N). Conversely, at temperatures between 1200–1500 ℃, the carbonaceous matter exhibited negligible amounts of hydrogen, sulfur, and nitrogen, primarily comprising carbon and oxygen. At higher temperatures (>1500 ℃), an increased breakdown of oxygen-containing functional groups occurred, leading to a reduction in oxygen content and an increase in carbon content in the carbonaceous matter, hence, CO content in the gas rose during this stage. At 1900 ℃, the carbon content of the residual char reaches 98.10 %.

Therefore, 1200 ℃ represents the pivotal temperature for carbon element purification, with the carbon content reaching 92.56 %. Further carbon enrichment requires a temperature over 1600 ℃. However, the operating temperature must be carefully evaluated considering the capacity and energy consumption of industrial carbonization equipment. Additionally, excessively high temperature is bound to decrease the reactivity of coal char. For gasification or metallurgical coke, the optimal temperature should not exceed 1200 ℃.

3.2. *Char morphology and porosity*

The evolution of particle surface morphology can be regarded as a

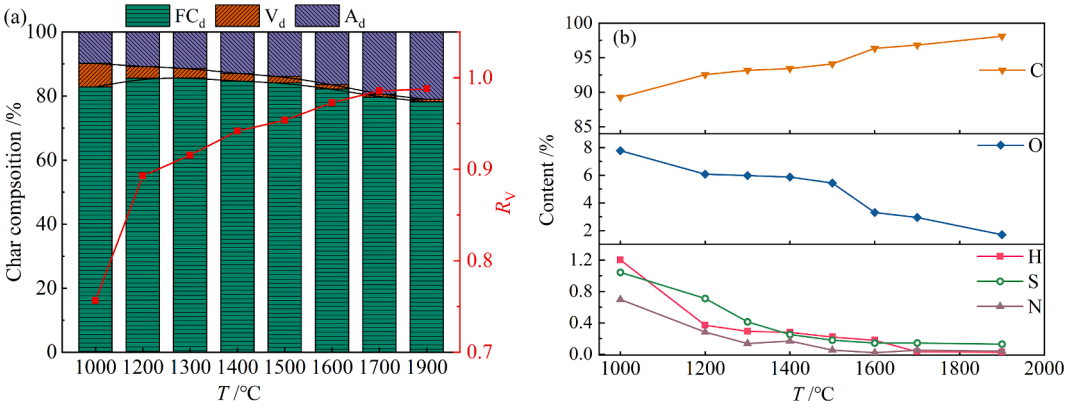

Fig. 3. Composition (a) and major elements content (b) of pyrolytic char at different temperatures.

reflection of the degree of carbonization of the pyrolytic coal char, and the morphology results at different temperatures are shown in Fig. 4. The surface of raw coal exhibited a rough and irregular texture, with distinct contour lines and a dense structure. When subjected to the high-temperature thermal shock, the particle surface gradually smoothened, showing clear carbon and ash distribution. Nonetheless, the overall morphology and structure remained relatively intact at temperatures below 1400 ℃. Above 1400 ℃, the char particle surface shows the grooves and striated texture, accompanied by a layered fiber-like distribution, possibly associated with the relatively thorough pyrolysis and graphitization transition within this temperature range [40,41]. Furthermore, the high-temperature thermal shock and release of volatiles induced the formation of numerous irregular pores and cracks on the particle surface. The mineral components were exposed on the char surface, which further melted and adhered to the particle surface with increasing temperature.

The detailed char structure data of the samples can be further obtained through the variation of surface area (S_{total}), pore volume (V_{total}), and pore size (d_{avg}), and the results are shown in Fig. 5. The original coal had a large average pore diameter, along with a small pore volume and surface area, indicating the dominance of mesopores and macropores in the pore structure. Conversely, the pores in the pyrolysis coal char were significantly developed after thermal shock, resulting in a decuple increase in the surface area and pore volume compared to the raw. Meanwhile, the average pore size decreased, indicating the exposure of micropores due to the release of volatile compounds during high-temperature pyrolysis. As the temperature increased, the average pore size generally trended upwards, showing that higher temperatures were conducive to the release of volatile matter and pore expansion. However, the pore volume and surface area displayed a trend of rapid increase followed by a gradual decrease with increasing temperature. The turning point coincided with the ash flow temperature (AFT = 1308 ℃). Above 1200 ℃, a rapid decline in pore volume and surface area was observed, along with a slight decrease in the average pore size. This phenomenon is attributed to the physical and chemical condensation of the remaining char structure and ash melting, which causes the blockage and disappearance of micropores [42,43].

In addition, the relative reduction in pore volume was smaller than the decrease in the surface area with the further increased temperature, and the pore volume slightly increased at higher temperatures (>1700 ℃). This indicated that higher temperature thermal shock caused pore expansion in coal char, elevating the total pore volume, as the micropores provide the main surface area. The destruction of micropores implies a reduction in the number of reactive active sites, which is detrimental to the reaction.

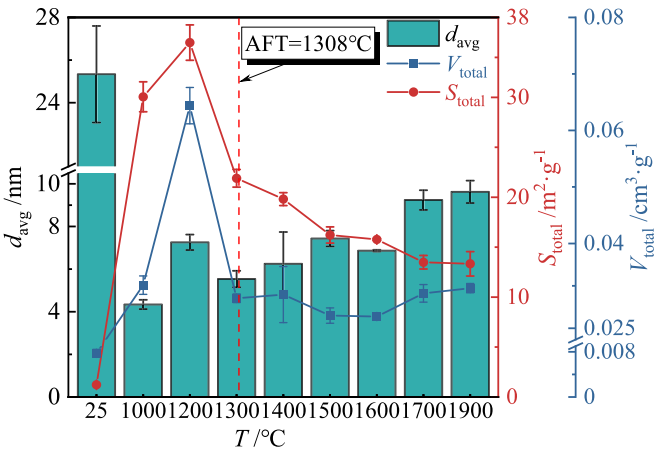

Fig. 5. Variation of pore parameters of coal char at different pyrolysis temperatures.

3.3. Carbon structure evolution

3.3.1. XRD analysis

The XRD patterns presented in Fig. 6 show the carbon structural evolution after thermal shock at different temperatures. Raw coal exhibited an amorphous property and did not display distinct diffraction peaks characteristic of graphite crystals in XRD analysis. Only faint graphite diffraction peaks at approximately 24.1° and 43.3° were observed, showing the presence of a minimal amount of microcrystalline structure within the raw material. Additionally, the crystalline peaks observed in the XRD spectra of the raw coal included the intrinsic mineral components, such as quartz.

After pyrolysis at 1000 ℃, two weak and broad graphite diffraction peaks were observed at 2θ of 24.9° and 43.0°, corresponding to the (002) and (100) crystal planes of the graphite microcrystal [44]. However, the intensity of the peaks remained low until reaching a temperature of 1300 ℃, indicating minimal growth and content of graphite microcrystals at this stage. Notably, during this stage, the (002) peak underwent a significant rightward shift, providing evidence for the transition from amorphous carbon to disordered graphitic carbon. Based on the aforementioned results, during this stage of pyrolysis, the primary process involved the release of volatiles. Although the

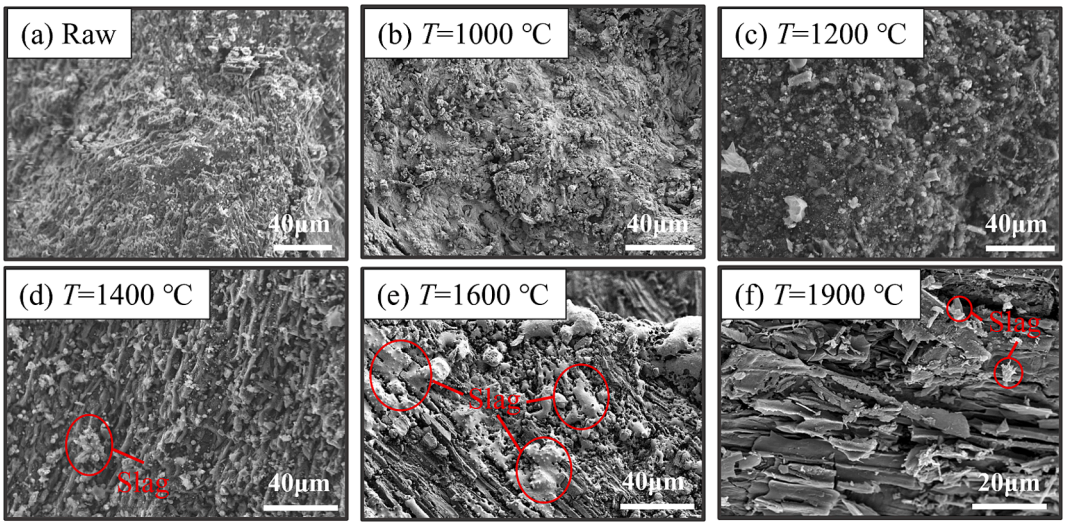

Fig. 4. Surface microstructure variation of char particles at different temperatures.

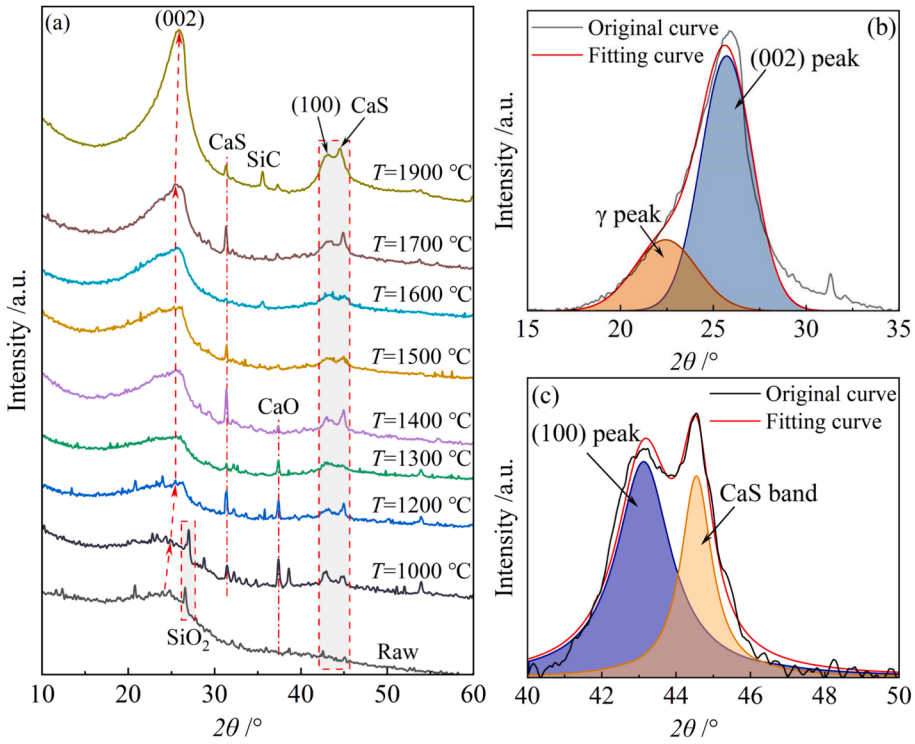

Fig. 6. (a) XRD patterns of coal char at different temperatures; (b) and (c), the split-peak fitting process.

carbon structure underwent deepening graphitization, there was minimal growth or formation of graphite crystals. During the temperature range of 1400–1600 ℃, the (0 0 2) peak shows a broad peak, showing the formation of nanoscale graphite crystallite. Upon further increase in pyrolysis temperature (>1700 ℃), the intensity and sharpness of the graphite peaks increased, accompanied by a rightward shift in the position of the (0 0 2) peak, indicating the growth of graphite structure; the peak shape tended to become more symmetric, which is the result of the decomposition of functional groups and the ordering of the carbon structure. The phenomena is similar to the previous study [21,26,45]. At higher pyrolysis temperatures (1900 ℃), the coal char exhibits heightened intensity of characteristic graphite-like peaks, including those corresponding to the (1 0 0) crystal planes of planar graphite.

Besides, during the pyrolysis process, volatiles precipitated and the relative content of ash increased. Previous studies have shown that the mineral compositions in raw coal are anhydrite and quartz [46]. As depicted in Fig. 4, the mineral components were exposed and melted on the surface, leading to the formation of slag pellets. With the increased temperature, characteristic peaks of the intrinsic mineral phases became evident in the XRD patterns. At 1000 ℃, the main crystalline phase was similar to the original coal minerals, primarily consisting of quartz, but with the appearance of CaO and oldhamite (CaS) crystals produced by the decomposition and carbothermal reactions of anhydrite. Subsequently, as the temperature surpassed 1400 ℃, exceeding the ash flow temperature (1308 ℃), the molten minerals reacted with CaO to form eutectics. At 1900 ℃, quartz underwent a carbothermal reaction with the carbon in the coal coke, resulting in the formation of SiC crystals and CO, which has a thermodynamically spontaneous reaction above 1789 K [39].

The assessment of the structure information of graphite microcrystals is based on the intensity of the (0 0 2) peak, whereas the condensation degree of aromatic structures is evaluated through the intensity of the (1 0 0) peak. Influenced by the presence of aliphatic hydrocarbon chains and various functional groups, the asymmetric broad peak at approximately 25.7° is considered to be the result of the overlapping of the (0 0 2) peak and the γ peak. Similarly, the peak at around 44° is the (1 0 0) crystallographic peak. The corresponding parameters such as peak positions, diffraction intensities, and half peak widths can be obtained from the peak splitting fits of Fig. 6 (b) and (c), as shown in Table 3. Also, the structural parameters (L_a, L_c, d_{002}, f_a) versus pyrolysis temperature are listed in Fig. 7.

As shown in Fig. 7, the interlayer spacing d_{002} gradually decreased with the increasing thermal shock temperatures, potentially due to the detachment of side chains and the aromatization of carbonaceous matter, leading to the formation of larger graphite structures. A further decrease in layer spacing occurred primarily at temperatures exceeding 1600 ℃, indicating the continued coalescence of aromatic ring lamellae under higher temperature thermal shock and the microcrystalline structure demonstrated a tendency towards ordered graphitization. Besides, the scales (L_a, L_c) of the microcrystals increased with temperature, yet the increase within the range of 1200–1600 ℃ is not substantial. It means that the size of graphite microcrystals experienced limited growth during this stage. However, L_a and L_c exhibited rapid growth beyond 1600 ℃, coinciding with the interval where interlayer spacing decreased. The observation suggests a critical transition in graphite microcrystals near 1600 ℃, and the carbonaceous matter in coal char was obviously transformed to ordered graphite. Notably, the lateral size (L_a) of graphite microcrystals exhibited a higher growth rate compared to the stacking height (L_c) below 1600 ℃. This phenomenon

Table 3
Carbon structural parameters of pyrolysis char under different temperatures after peak-fitting of XRD patterns.

T /℃	$2\theta_{(002)}$/°	$\beta_{(002)}$/°	$A_{(002)}$/%	$2\theta_{(100)}$/°	$\beta_{(100)}$/°
25	24.10	4.84	37.71	43.26	10.87
1000	24.91	4.35	51.66	42.95	2.27
1200	25.49	4.16	52.62	42.93	1.95
1300	25.50	4.08	53.59	42.83	1.90
1400	25.55	4.02	55.66	42.99	1.80
1500	25.62	3.92	56.88	42.99	1.77
1600	25.64	3.85	58.00	43.26	1.74
1700	25.65	3.57	63.95	43.02	1.58
1900	25.90	3.26	74.64	43.03	1.43

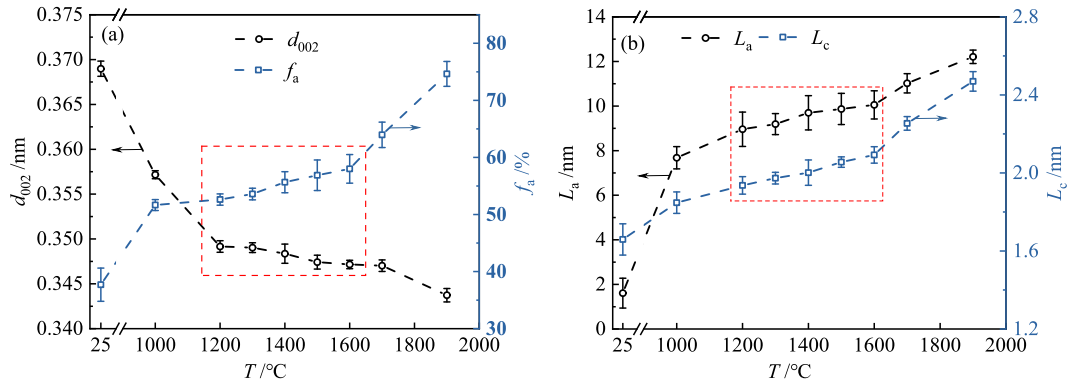

Fig. 7. Relationships between the structural parameters from XRD results and temperatures.

can be attributed to the inhibitory effect caused by the presence of side chains and heteroatom components in coal char, which impede the vertical stacking of graphite microcrystals. The formation of new aromatic structures between graphite microcrystals through aromatization contributed to an increase in the size of graphite microcrystals but did not favor the formation of a three-dimensional graphite structure. However, at higher temperatures (>1600 ℃), the growth rate of L_a was lower than that of L_c. It can be attributed to the transformation of aliphatic groups and the elimination of heteroatoms situated between graphite layers, facilitating the stacking of graphite layers.

In addition, the degree of graphitization of the samples below 2000 ℃ was assessed using aromaticity (f_a), which quantifies the relative content of aliphatic carbon atoms, including aliphatic hydrocarbon branched chains, alicyclic hydrocarbons, and carbon-containing functional groups [2,33]. As the temperature increased, f_a rose from an initial value of 38.3 % and reached 77.6 % at 1900 ℃. indicating an enhanced level of pyrolysis and the growth of graphite microcrystals. Additionally, at lower temperatures (<1600 ℃), the increment rate of f_a was slower and a proportion of aliphatic carbon atoms persisted. Combined with the oxygen content results in Fig. 3(b), it can be surmised that the smaller variation of f_a is related to the presence of carbonyl and heterocyclooxy functional groups. The presence of attached aliphatic carbon and heteroatoms in graphite structure also hindered the stacking and growth of aromatic sheets [21]. The result aligned with the relationship between the variation of L_a and L_c. Moreover, f_a demonstrates a notable increase above 1600 ℃, providing evidence of intensified pyrolysis of coal char and an increased level of graphitization.

3.3.2. *Raman spectroscopy analysis*

Raman reflects the vibrational modes of the carbon molecules, and the pyrolysis char results are shown in Fig. 8. Typical Raman vibration peaks of raw coal were observed at 1350 cm^{-1} (representing the sp^3 bond or sp^2 bond of hybridization defects) and 1580 cm^{-1} (representing the sp^2 bond). Similar peak shapes and intensities were observed at various positions, which proved the uniformity of the carbon structure on the surface of the original coal particles. After the thermal shock, the intensity of the D peak increased while the G peak decreased on the surface of the coal char. It can be attributed to the structural disruption of coal particles, resulting in the formation of a fragmented structure on the surface and an increase in defective carbon structures. Additionally, the 2D peak emerged at 2660 cm^{-1} after thermal shock, which is a characteristic peak associated with ordered graphite [44,47]. Especially at temperatures above 1600 ℃, the intensity of the peak increased significantly, proving the trend of transition from disordered carbon to ordered graphite. While, in this study, the peak position displayed asymmetry and a slight shift towards lower frequencies, attributed to the interaction between different layers present in multilayer graphite.

Raman intensity is influenced by a variety of factors, including the light absorptivity and Raman scattering ability of coal [2]. It is difficult

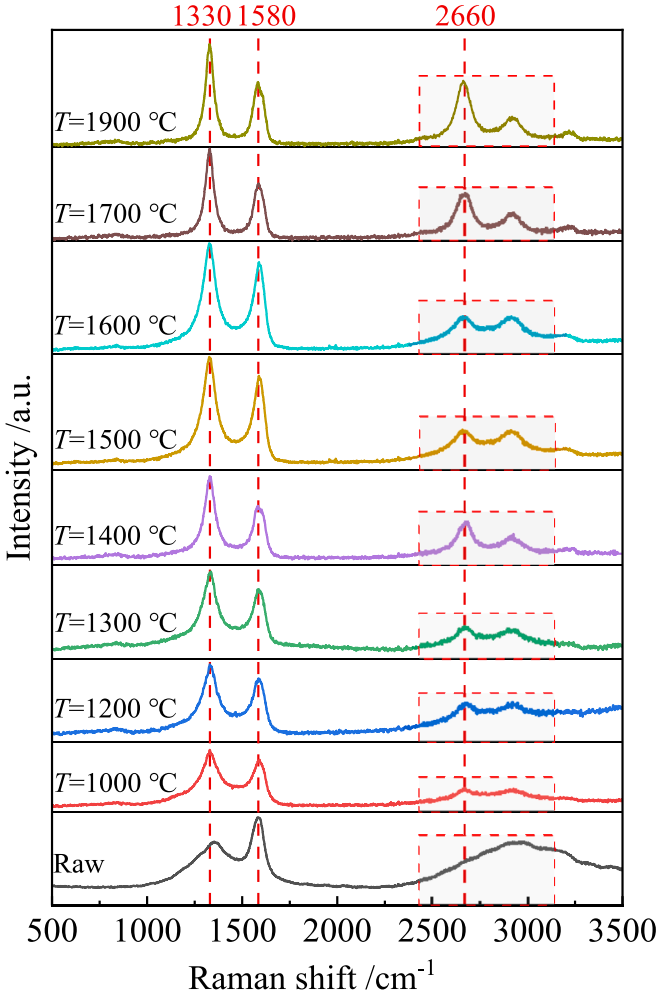

Fig. 8. Raman spectra of the raw and the pyrolysis coal particles at different temperatures.

to infer the differences in the carbon structure from the variations in peak intensities. Hence, the D and G peaks of Raman spectra were fitted with Lorentzian and Gaussian functions, respectively, and the split-peak fitting results are shown in Fig. 9. Parameters such as peak position, bands, Raman shift, and vibration modes used in this study are shown in Table 4.

The evolution of the carbon structure throughout the entire temperature stage followed a similar pattern to the composition variation. Below 1600 ℃, the percentage of the G peak area exhibited a slight

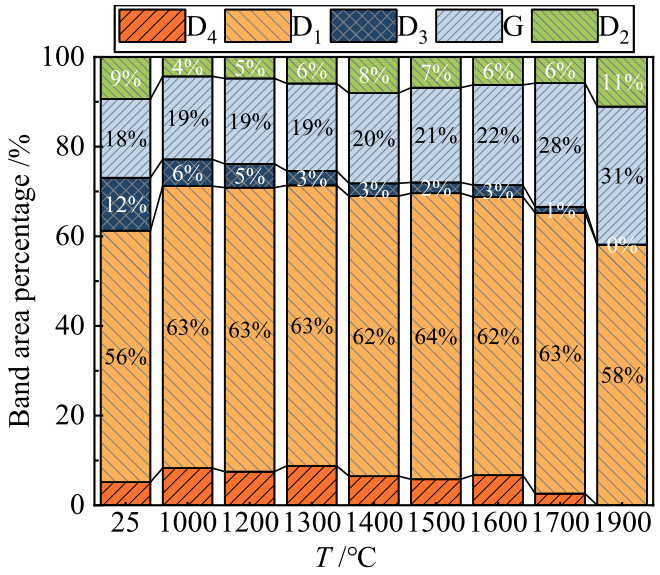

Fig. 9. The band area proportion in carbon structure at different temperatures.

Table 4
First-order Raman bands, Raman shift, and vibration modes used in this study [47,48].

Band	Raman shift/ cm^{-1}	Vibration mode
G	~1580	Ideal graphite lattice (E_{2g} symmetry)
D_1	~1350	Disordered graphitic lattice (graphene layer edges, A_{1g} symmetry)
D_2	~1620	Disordered graphitic lattice (surface graphene layers, E_{2g}-symmetry)
D_3	~1500	Amorphous carbon
D_4	~1200	Disordered graphitic lattice (A_{1g} symmetry), polyenes, ionic impurities

increase. D_1 remained nearly unchanged during 1200–1600 ℃, but a slight increase compared to the raw coal, demonstrating an increase in disordered graphite lattice, which is attributed to the transformation of amorphous carbon (Table 4). D_3 continued to decrease, and D_4 slightly decreased. The results suggest that the primary thermochemical changes occurring in the coal at this stage involved the transformation of aliphatic compounds and aromatic side-chain structures, as well as the release of olefinic and ionic impurities from the interlayers of graphite in a gaseous state. During 1200–1600 ℃, the total disordered graphite carbon content was unaffected, suggesting that the decrease in reactivity during this stage was insignificant [21,33]. At temperatures above 1600 ℃, the percentage of the G peak displayed a substantial increase, while the D_1, D_3, and D_4 peaks experienced decreases. Combined with Table 4, this pattern indicated a reduction in the content of amorphous carbon (D_3) within this temperature range, accompanied by the gradual ordering of the disordered graphite lattice, hence, graphite microcrystalline further grows. The increased ordering of the carbon structure reduces the reactivity, which is detrimental to the reaction [16,17]. Throughout the entire temperature interval, the proportion of D_2 peaks exhibited an overall increasing trend, indicating that the thermal shock caused damage to the surface of the graphite lattice.

The relationship between carbonaceous structural parameters and temperature is shown in Fig. 10. Generally, the variation of $(I_{D3}+I_{D4})/I_G$ is attributed to variations in the amorphous carbon, disordered graphite lattice, and ionic impurities, reflecting alterations in cross-linking density and the number of substituent groups [47,48]. It was used as a criterion for assessing the level of carbonization in the coal char in this study. The ratio of I_{D1}/I_G reflects changes in the average size of graphite

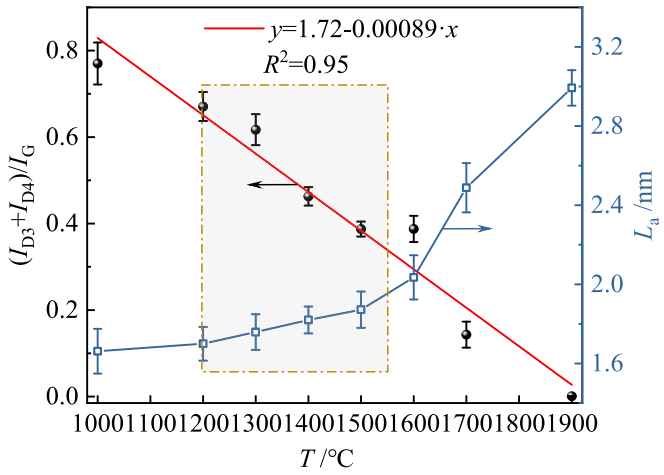

Fig. 10. Relationships between the structural parameters from Raman spectrum results and temperature.

microcrystals. and the average crystallite lateral size (L_a) of carbon microcrystals can be further calculated based on Eq. (5).

Within the experimental temperature range, $(I_{D3}+I_{D4})/I_G$ consistently decreased as the temperature increased, indicating the occurrence of cross-linking and polycondensation reactions, as well as the transformation of the amorphous carbon structure and an increase in the degree of carbonization. Furthermore, a nearly linear relationship between $(I_{D3}+I_{D4})/I_G$ and the temperature was observed in the range of 1000–1900 ℃, proving the purification of the carbon matrix increased linearly. The fitting equation, with an R^2 of 0.95, is presented in Fig. 10. Additionally, the transformation process of graphite microcrystals can be analyzed by L_a. The results show that the growth of graphite microcrystals was not obvious within the temperature range of 1000–1600 ℃, and L_a gradually increased from 1.66 to 2.03 nm. However, at higher temperatures (>1600 ℃), the size of graphite microcrystals exhibited rapid growth, and this phenomenon was consistent with the result obtained from XRD analysis.

3.3.3. *Local structural evolution*

The micromorphology and nanostructures of coal particles at various temperatures are shown in Fig. 11, and more results are listed in Fig. S2 in the Supplementary materials. As shown in Fig. 11(II) of (a)~(d), under thermal shock at 1000 ℃, the coal char exhibited abundant edge defect structures and amorphous carbon. As the temperature increased, the length of basic structural units increased slightly, and the stacking layer and the edge contour became more obvious. At 1900 ℃, a lamellar structure similar to the graphite layer could be observed.

The microcrystalline structures in the carbonaceous matter are shown in Fig. 11(I) of (a)~(d). At a lower temperature (1000 ℃), the carbon structure in coal char primarily manifested as amorphous, with a small amount of disordered graphitic microcrystalline structure exhibiting random orientation. As the temperature increased, graphite microcrystals continued to grow and amalgamate, forming a series of aromatic flakes with parallel stripes. However, at the experimental temperature, a substantial number of aromatic flake stacks displayed randomness and disordered distribution. Within the temperature range of 1000–1900 ℃, the layer spacing of graphite microcrystals slightly decreased with increasing temperature (Fig. 11(III)), the number of stacked layers decreased, and the degree of order exhibited an increasing trend. Higher temperatures (1900 ℃) showed semi-ring structural features, and some basic structural units appear, which consist of some graphite crystallites oriented in a wavy pattern, and the layer spacing decreases. Notably, the structure of graphite microcrystals underwent no significant transformation in the temperature range of 1200–1600 ℃. Instead, the temperature elevation primarily led to the

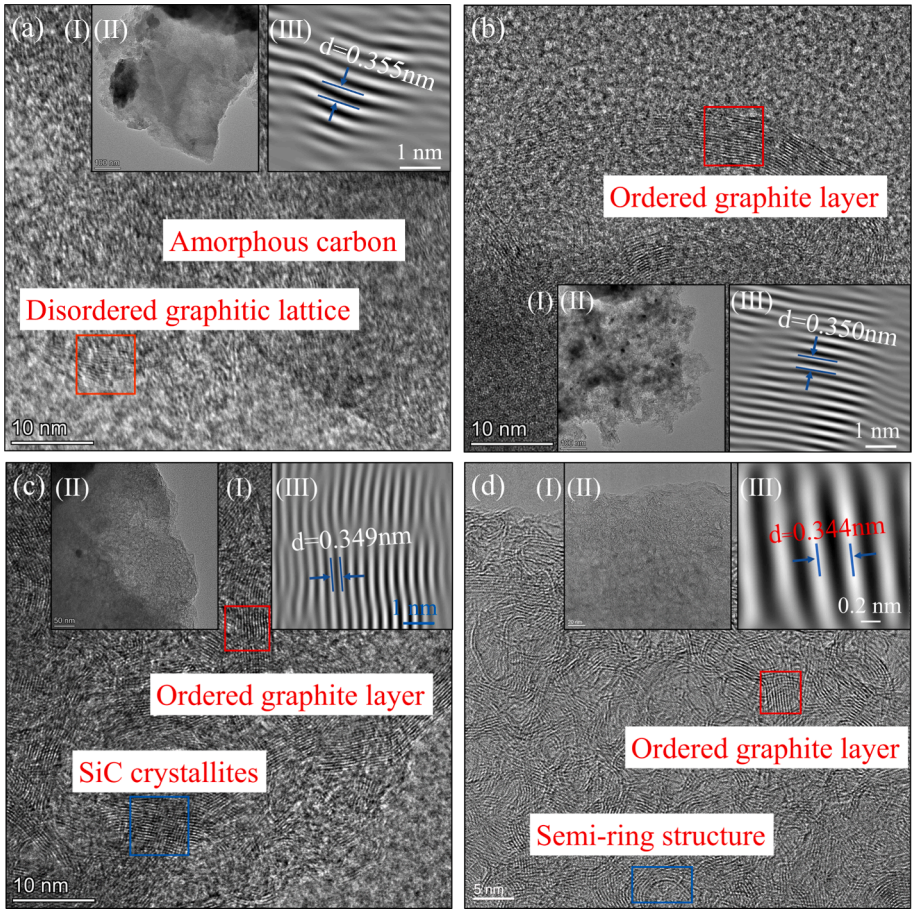

Fig. 11. HRTEM (I) and TEM (II) micrographs and the corresponding nanostructures graphs (III) of char samples at different temperatures, (a), at 1000 ℃; (b), at 1200 ℃; (c), at 1600 ℃; (d), at 1900 ℃.

generation of more randomly distributed graphite microcrystals [10]. The result indicated that, within this temperature interval, the growth and ordering of graphite microcrystals were minimally affected, and primarily involved the transformation of disordered carbon and the removal of aliphatic compounds.

3.4. Pyrolysis process and mechanism

The schematic of the high-temperature pyrolytic process and mechanism of bituminous coal under thermal shock is shown in Fig. 12. In the temperature range of 1000–1900 ℃, the pyrolytic process can be summarized as the elimination of heteroatoms and the formation of an aromatic carbon skeleton. It can be further divided into two stages. During 1000–1500 ℃, aliphatic transforms into aromatic, and depolymerization and aromatization lead to the amorphous carbon being converted into a disordered layered graphite structure. As the pyrolysis temperature increased, micropores and cracks emerged, releasing a significant amount of small molecule gaseous products. The formation of gas-phase products is attributed to a free radical reaction process, and the elevated pyrolysis temperature intensified the breakage of weak bridging bonds in char, leading to an increased degree of aromatization of aliphatic compounds [49]. It also enhanced the carbonaceous purity and the concentration of CO and hydrogen in the gas. Notably, even with an increased pyrolysis temperature in this range, the graphite microcrystals maintained a disordered layer structure and exhibited random orientation on the nanoscale, making it challenging to order. This stage is

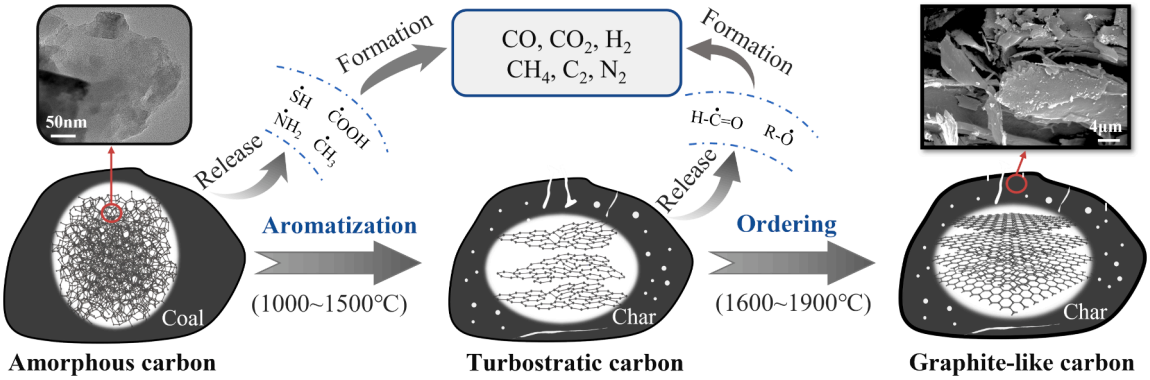

Fig. 12. Schematic of high-temperature pyrolysis process and mechanism.

conducive to the removal of heteroatoms in the carbonaceous matter, and the carbon content in the coal char can exceed 90 %, with relatively little impact on the reactivity due to the presence of randomly arranged graphite microcrystals instead of ordering.

In the higher temperature stage (1600–1900 ℃), the disordered graphitized carbon showed an ordered arrangement. Graphite microcrystals grow along the edges, and part of microcrystalline structures are reoriented and connected to form local graphite-like nanostructures. In this stage, the surface structure of coal char had significant variation, gradually forming a flake texture, even though it does not have regular graphite layers like true graphite. Simultaneously, strong bonds (ethers or aldehydes) were broken, leading to a slight increase in gas-phase products, primarily in the form of elevated CO content. The degree of aromatization in the coal char significantly increased, the size of the microcrystals rapidly increased, and it was significantly influenced by temperature. This stage is favorable for the preparation of precursors of carbon materials from coal char but is unfavorable for the preparation of metallurgical char or power coal char.

4. Conclusions

This study investigated the pyrolysis characteristics and the evolution of microstructures of bituminous coal particles, under thermal shock conditions ranging from 1000 to 1900 ℃. A modified flash Joule heating equipment was used to realize this process. In the experimental temperature range, the purification of the coal char is a successive process linear on temperature. While the carbon structure evolution could be divided into two distinct stages. Specifically, below 1600 ℃, the transformation of amorphous carbon into disordered graphite is primary. During this stage, heteroatoms and side chains are released as gas products, and depolymerization and aromatization lead to the formation of small-sized aromatic structures. Nevertheless, no significant alterations were presented in terms of particle morphology and graphite microcrystalline size. The temperature range of 1600–1900 ℃ is a critical interval for the formation of graphite-like structure, heteroatoms (O) are further eliminated, and the gas (CO) product yield increases. Further condensation facilitated the growth and coalescence of graphite microcrystals, evidenced by the increased crystal size and ordering in orientation. While this stage facilitates subsequent investigations on carbon materials, but leads to reduced char reactivity.

CRediT authorship contribution statement

Haigang Zhang: Writing – review & editing, Writing – original draft, Software, Methodology, Investigation, Data curation, Conceptualization. **Zhongjie Shen:** Writing – review & editing, Supervision, Project administration, Methodology, Funding acquisition, Conceptualization. **Rubin Zeng:** Software, Methodology, Investigation, Data curation. **Qinfeng Liang:** Writing – review & editing, Visualization, Supervision, Investigation. **Haifeng Liu:** Writing – review & editing, Supervision, Resources, Conceptualization.

Declaration of competing interest

The authors declare that they have no known competing financial interests or personal relationships that could have appeared to influence the work reported in this paper.

Data availability

The authors are unable or have chosen not to specify which data has been used.

Acknowledgments

This study is supported by the National Natural Science Foundation of China (22378130), National Key R&D Program of China (2022YFC3902502-04), Key R&D Program of Xinjiang Uygur Autonomous Region (2022B03026-1), the Fundamental Research Funds of the Central Universities (2022ZFJH004).

Appendix A. Supplementary material

Supplementary data to this article can be found online at https://doi.org/10.1016/j.fuel.2024.132096.

References

[1] Dziejarski B, Krzyżyńska R, Andersson K. Current status of carbon capture, utilization, and storage technologies in the global economy: a survey of technical assessment. Fuel 2023;342:127776.
[2] Li K, Cao H, Rimmer SM, Zhang H, Li X, Zhang Y, et al. Petrographic features and carbon structural evolution of a series of high-temperature treated anthracites. Int J Coal Geol 2023;277:104356.
[3] Yadav S, Mondal SS. A complete review based on various aspects of pulverized coal combustion. Int J Energy Res 2019;43:3134–65.
[4] Yang W, Wang Y, Yan F, Si G, Lin B. Evolution characteristics of coal microstructure and its influence on methane adsorption capacity under high temperature pyrolysis. Energy 2022;254:124262.
[5] Zhang S, Lu J, Zhang J, Yue G. Effect of pyrolysis intensity on the reactivity of coal char. Energy Fuels 2008;22:3213–21.
[6] Chen T, Zhang K, Zheng M, Yang S, Yellezuome D, Zhao R, et al. Thermal properties and product distribution from pyrolysis at high heating rate of Naomaohu coal. Fuel 2021;292:120238.
[7] Jaiswal S, Singh R, Singh V, Mukherjee AK. A study of the effects of thermal shocks on liberation characteristics of high coal ash particles. Fuel 2018;233:215–23.
[8] Chen H, Wang S, Zhang X, Zhao Y, Zhang H. A study of chemical structural evolution of thermally altered coal and its effect on graphitization. Fuel 2021;283:119295.
[9] Feng B, Bhatia SK, Barry JC. Structural ordering of coal char during heat treatment and its impact on reactivity. Carbon 2002;40:481–96.
[10] Zhang S, Liu Q, Zhang H, Ma R, Li K, Wu Y, et al. Structural order evaluation and structural evolution of coal derived natural graphite during graphitization. Carbon 2020;157:714–23.
[11] Ding L, Gong Y, Wang Y, Wang F, Yu G. Characterisation of the morphological changes and interactions in char, slag and ash during CO_2 gasification of rice straw and lignite. Appl Energy 2017;195:713–24.
[12] Yu J, Guo Q, Ding L, Gong Y, Yu G. Studying effects of solid structure evolution on gasification reactivity of coal chars by in-situ Raman spectroscopy. Fuel 2020;270:117603.
[13] Xu K, Hu S, Zhang L, Li H, Chen Y, Xiong Z, et al. Effect of temperature on Shenfu coal pyrolysis process related to its chemical structure transformation. Fuel Process Technol 2021;213:106662.
[14] Lv X, Zhang T, Luo Y, Zhang Y, Wang Y, Zhang G. Study on carbon nanotubes and activated carbon hybrids by pyrolysis of coal. J Anal Appl Pyrol 2020;146:104717.
[15] Jiang Y, Zong P, Tian B, Xu F, Tian Y, Qiao Y, et al. Pyrolysis behaviors and product distribution of Shenmu coal at high heating rate: a study using TG-FTIR and Py-GC/MS. Energy Convers Manag 2019;179:72–80.
[16] Surup GR, Nielsen HK, Heidelmann M, Trubetskaya A. Characterization and reactivity of charcoal from high temperature pyrolysis (800–1600 °C). Fuel 2019;235:1544–54.
[17] Zhao C, Ge L, Li X, Zuo M, Xu C, Chen S, et al. Effects of the carbonization temperature and intermediate cooling mode on the properties of coal-based activated carbon. Energy 2023;273:127177.
[18] Russell NV, Gibbins JR, Man CK, Williamson J. Coal char thermal deactivation under pulverized fuel combustion conditions. Energy Fuels 2000;14:883–8.
[19] Oberlin A. Carbonization and graphitization. Carbon 1984;22:521–41.
[20] Li J, Qin Y, Chen Y, Song Y, Wang Z. HRTEM observation of morphological and structural evolution of aromatic fringes during the transition from coal to graphite. Carbon 2022;187:133–44.
[21] Zhang X, Wang S, Chen H, Wang X, Deng J, Li X, et al. Observation of carbon nanostructure and evolution of chemical structure from coal to graphite by high temperature treatment, using componential determination, X-ray diffraction and high-resolution transmission electron microscope. Fuel 2023;332:126145.
[22] Jiang X, Xu J, He Q, Wang C, Jiang L, Xu K, et al. A study of the relationships between coal heterogeneous chemical structure and pyrolysis behaviours: mechanism and predicting model. Energy 2023;282:128715.
[23] Zhang L, Wang G, Xue Q, Zuo H, She X, Wang J. Effect of preheating on coking coal and metallurgical coke properties: a review. Fuel Process Technol 2021;221:106942.
[24] Du M, Advincula PA, Ding X, Tour JM, Xiang C. Coal-based carbon nanomaterials: en route to clean coal conversion toward net zero CO2. Adv Mater 2023. n/a:2300129.
[25] Zang X, Dong Y, Jian C, Ferralis N, Grossman JC. Upgrading carbonaceous materials: coal, tar, pitch, and beyond. Matter 2022;5:430–47.
[26] Huang P, Zhu R, Zhang X, Zhang W. Effect of free radicals and electric field on preparation of coal pitch-derived graphene using flash Joule heating. Chem Eng J 2022;450:137999.

[27] Gai L, Li J, Wang Q, Tian R, Li K. Evolution of biomass to porous graphite carbon by catalytic graphitization. J Environ Chem Eng 2021;9:106678.
[28] Dıez MA, Alvarez R, Barriocanal C. Coal for metallurgical coke production: predictions of coke quality and future requirements for cokemaking. Int J Coal Geol 2002;50:389–412.
[29] Wall TF, Lowe A, Wibberley LJ, Stewart IM. Mineral matter in coal and the thermal performance of large boilers. Prog Energy Combust Sci 1979;5:1–29.
[30] Pereira EG, da Silva JN, de Oliveira JL, Machado CS. Sustainable energy: a review of gasification technologies. Renew Sustain Energy Rev 2012;16:4753–62.
[31] Lu L, Sahajwalla V, Kong C, Harris D. Quantitative X-ray diffraction analysis and its application to various coals. Carbon 2001;39:1821–33.
[32] Schito A, Muirhead DK, Parnell J. Towards a kerogen-to-graphite kinetic model by means of Raman spectroscopy. Earth Sci Rev 2023;237:104292.
[33] Zeng H, Xing B, Cao Y, Xu B, Hou L, Guo H, et al. Insight into the microstructural evolution of anthracite during carbonization-graphitization process from the perspective of materialization. Int J Min Sci Technol 2022;32:1397–406.
[34] Thommes M, Kaneko K, Neimark AV, Olivier JP, Rodriguez-Reinoso F, Rouquerol J, et al. Physisorption of gases, with special reference to the evaluation of surface area and pore size distribution (IUPAC Technical Report). Pure Appl Chem 2015;87:1051–69.
[35] Jiang Y, Zong P, Ming X, Wei H, Zhang X, Bao Y, et al. High-temperature fast pyrolysis of coal: an applied basic research using thermal gravimetric analyzer and the downer reactor. Energy 2021;223:119977.
[36] Sun S, Xu D, Wei Y, Zhi Y, Jiang G, Guo Y. Influence laws of operating parameters on coal pyrolysis characteristics. J Anal Appl Pyrol 2022;167:105684.
[37] Zhang H, Shen Z, Dong Z, Yang Y, Xu J, Liang Q, et al. Experimental study on the effect of temperature and oxygen on pyrolysis-gasification decoupling characteristics of Yili coal. J Anal Appl Pyrol 2023;172:106007.
[38] Gao R, Dou B, Chang Q, Xu J, Dai Z, Yu G, et al. Effect of temperature and hydrogen on product distribution and evolution of char structure during pyrolysis of bituminous coal in a drop tube furnace. Fuel 2020;267:117078.
[39] Kong J, Gao S, Liu Y, Jin X, Wei D, Jiang S, et al. Recycling of carbonized rice husk for producing high purity silicon by the combination of electric arc smelting and slag refining. J Hazard Mater 2019;380:120827.
[40] Shu X, Xu X. Study on morphology of chars from coal pyrolysis. Energy Fuels 2001; 15:1347–53.
[41] Zhong M, Gao S, Zhou Q, Yue J, Ma F, Xu G. Characterization of char from high temperature fluidized bed coal pyrolysis in complex atmospheres. Particuology 2016;25:59–67.
[42] Xiao J, Li F, Zhong Q, Huang J, Wang B, Zhang Y. Effect of high-temperature pyrolysis on the structure and properties of coal and petroleum coke. J Anal Appl Pyrol 2016;117:64–71.
[43] Li S, Whitty KJ. Investigation of coal char−slag transition during oxidation: effect of temperature and residual carbon. Energy Fuels 2009;23:1998–2005.
[44] Zhang S, Song B, Cao C, Zhang H, Liu Q, Li K, et al. Structural evolution of high-rank coals during coalification and graphitization: X-ray diffraction, Raman spectroscopy, high-resolution transmission electron microscopy, and reactive force field molecular dynamics simulation study. Energy Fuels 2021;35:2087–97.
[45] Vázquez-Santos MB, Martínez-Alonso A, Tascón JMD, Rouzaud J-N, Geissler E, László K. Complementary X-ray scattering and high resolution imaging of nanostructure development in thermally treated PBO fibers. Carbon 2011;49: 2960–70.
[46] Zhang H, Shen Z, Liang Q, Xu J, Guo X, Dai Z, et al. Micro-scale study of mineral transformation and coverability at single coal char particle surface during high-temperature gasification process. Fuel 2024;358:130249.
[47] Sadezky A, Muckenhuber H, Grothe H, Niessner R, Pöschl U. Raman microspectroscopy of soot and related carbonaceous materials: spectral analysis and structural information. Carbon 2005;43:1731–42.
[48] Tuinstra F, Koenig JL. Raman spectrum of graphite. J Chem Phys 1970;53: 1126–30.
[49] Liu P, Zhang D, Wang L, Zhou Y, Pan T, Lu X. The structure and pyrolysis product distribution of lignite from different sedimentary environment. Appl Energy 2016; 163:254–62.